# Not too big, not too small: the dark haloes of the dwarf spheroidals in the Milky Way

Vera-Ciro, Carlos A.; Helmi, Amina; Starkenburg, Else; Breddels, Maarten A.

*Published in:*
Monthly Notices of the Royal Astronomical Society

*DOI:*
10.1093/mnras/sts148



*Publication date:*
2013

Monthly Notices
of the
ROYAL ASTRONOMICAL SOCIETY

MNRAS **428,** 1696–1703 (2013) doi:10.1093/mnras/sts148

# Not too big, not too small: the dark haloes of the dwarf spheroidals in the Milky Way

Carlos A. Vera-Ciro,[1]⋆ Amina Helmi,[1] Else Starkenburg[1,2] and Maarten A. Breddels[1]

[1]*Kapteyn Astronomical Institute, University of Groningen, PO Box 800, 9700 AV Groningen, the Netherlands*
[2]*Department of Physics and Astronomy, University of Victoria, PO Box 3055, STN CSC, Victoria, BC V8W 3P6, Canada*

Accepted 2012 October 4. Received 2012 September 13; in original form 2012 February 27

## ABSTRACT

We present a new analysis of the Aquarius simulations done in combination with a semi-analytic galaxy formation model. Our goal is to establish whether the subhaloes present in Λ cold dark matter simulations of Milky Way (MW) like systems could host the dwarf spheroidal (dSph) satellites of our Galaxy. Our analysis shows that, contrary to what has been assumed in most previous work, the mass profiles of subhaloes are generally not well fitted by Navarro–Frenk–White models but that Einasto profiles are preferred. We find that for shape parameters $\alpha = 0.2$–$0.5$ and $v_{\rm max} = 10$–$30$ km s$^{-1}$ there is very good correspondence with the observational constraints obtained for the nine brightest dSphs of the MW. However, to explain the internal dynamics of these systems as well as the number of objects of a given circular velocity the total mass of the MW should be $\sim 8 \times 10^{11}$ M$_\odot$, a value that is in agreement with many recent determinations, and at the low-mass end of the range explored by the Aquarius simulations. Our simulations show important scatter in the number of bright satellites, even when the Aquarius MW-like hosts are scaled to a common mass, and we find no evidence for a missing population of massive subhaloes in the Galaxy. This conclusion is also supported when we examine the dynamics of the satellites of M31.

**Key words:** galaxies – halos cosmology – dark matter galaxies – Local Group galaxies – kinematics and dynamics.

## 1 INTRODUCTION

Despite the great success of the Λ cold dark matter (ΛCDM) concordance cosmological model on large scales, on the scales of galaxies and below the theory is often defied. Some of the issues on small scales have been consistently explained within the theory itself with the inclusion of physical processes that mostly affect baryons. This is the case for the 'missing satellite problem' (Klypin et al. 1999; Moore et al. 1999), namely the overabundance of satellites in dark matter only simulations compared to the observed number of luminous objects around the Milky Way (MW) and other nearby galaxies. It is now widely accepted that the shallow potential wells of small dark matter haloes must be strongly affected by reionization and feedback, making star formation highly inefficient in such systems (Couchman & Rees 1986; Efstathiou 1992; Kauffmann, White & Guiderdoni 1993; Thoul & Weinberg 1996; Bullock, Kravtsov & Weinberg 2000; Benson et al. 2002; Somerville 2002; Li et al. 2009; Okamoto & Frenk 2009; Macciò et al. 2010; Stringer, Cole & Frenk 2010; Font et al. 2011; Guo et al. 2011).

Recently, Boylan-Kolchin, Bullock & Kaplinghat (2011) have argued that the dark matter satellites (subhaloes hereafter) predicted by ΛCDM are persistently too dense to host the observed population of dwarf spheroidal (dSph) galaxies in the MW if these are embedded in haloes following Navarro, Frenk & White (1996, 1997, hereafter NFW) profiles. More recently, Boylan-Kolchin, Bullock & Kaplinghat (2012) presented an even stronger argument (free of the assumption of a specific density profile) and argued that the MW is missing a population of massive satellites. A few studies have been published in the literature that address this conundrum. Lovell et al. (2012) showed that in warm dark matter cosmological simulations of MW-like haloes, the circular velocity curves of subhaloes are consistent with the constraints derived by Wolf et al. (2010) for the MW satellites (see also Walker et al. 2009). Following a similar line, Vogelsberger, Zavala & Loeb (2012) carried out simulations of self-interacting dark matter and showed that the most massive subhaloes develop cores, what could partially solve the problem. On the other hand, Di Cintio et al. (2011) pointed out that by including baryons in the CDM context the problem becomes more severe probably due to the additional adiabatic contraction experienced by the dark matter subhaloes hosting gas.

There are two assumptions sometimes implicit in the models which may lead to biased answers if overlooked. These concern

⋆E-mail: cavera@astro.rug.nl

(i) the actual mass of the MW[1] and (ii) the density profiles followed by dark matter satellites assembled in ΛCDM. The first issue has been addressed with a plethora of methods leading to measures that, usually, are consistent with a total mass of $0.7–2.0 \times 10^{12}\,\mathrm{M}_{\odot}$ (Kochanek 1996; Wilkinson & Evans 1999; Sakamoto, Chiba & Beers 2003; Battaglia et al. 2005, 2006; Smith et al. 2007; Li & White 2008; Xue et al. 2008; Kallivayalil et al. 2009; Gnedin et al. 2010; Guo et al. 2010; Watkins, Evans & An 2010; Busha et al. 2011a). The measurements suffer from uncertainties in the modelling as well as limitations in the kinematics of the tracers used. Therefore, comparisons to simulations of MW dark matter haloes should take this uncertainty into account.

On the second issue, namely the density profile of subhaloes, significant progress has been made, especially in recent years. Already Stoehr et al. (2002) found that the circular velocity curves of subhaloes in cosmological *N*-body simulations are more narrowly peaked (in a log–log plot) than the widely used NFW models and explored how consistent these were with the internal kinematics of the MW satellites. The outstanding numerical resolution achieved in the latest of such cosmological *N*-body simulations has enabled a closer examination of the shape of the density profile down to the innermost few parsecs of dark matter haloes (Madau, Diemand & Kuhlen 2008; Springel et al. 2008). Such studies have shown that Einasto models provide better matches to the density profiles found in the simulations than the NFW form (Navarro et al. 2010; Reed, Koushiappas & Gao 2011; Di Cintio et al. 2012) confirming previous results on the subject (Navarro et al. 2004; Merritt et al. 2005, 2006; Graham et al. 2006; Prada et al. 2006; Gao et al. 2008).

In this paper, we will reconsider both these issues and establish how much they affect the conclusions drawn by Boylan-Kolchin et al. (2011, 2012). Like these authors we use the Aquarius haloes, but we supplement the dynamical information provided by the simulations with a semi-analytic galaxy formation model (Starkenburg et al. 2012). One of the advantages of this approach is that it enables us to directly compare objects in the simulation with those observed. We introduce some relevant features of the simulations in Section 2, while in Section 3 we present the results of our analysis in detail. We draw our conclusions in Section 4.

## 2 NUMERICAL PRELIMINARIES

We use the simulations of the Aquarius project, six MW-sized dark matter haloes assembled in a background cosmology consistent with the constraints yielded by *WMAP*1. Each halo (labelled from A to F) was simulated at different resolutions, starting from a particle mass ($m_{\mathrm{p}}$) of $3.143 \times 10^{6}\,\mathrm{M}_{\odot}$ for the lowest resolution to $1.712 \times 10^{3}\,\mathrm{M}_{\odot}$ for the highest resolution. In what follows, we focus on the level 2 which is the highest level at which *all* the Aquarius haloes were simulated (for more details see Springel et al. 2008).

Subhaloes in these simulations are identified as bound overdensities with SUBFIND (Springel et al. 2001). For each subhalo we compute the circular velocity profile as $v_{\mathrm{c}}^2(r) = Gm(r)/r$, where $m(r)$ is the mass enclosed within the spherical radius $r$. The maximum circular velocity $v_{\mathrm{max}}$ is defined as the peak of the circular velocity curve, and is reached at position $r_{\mathrm{max}}$, i.e. $v_{\mathrm{c}}(r_{\mathrm{max}}) = v_{\mathrm{max}}$.

Numerical convergence is established by looking at the convergence radius as defined by Power et al. (2003). Navarro et al. (2010) showed that the roots of the equation

$$\kappa = \frac{\sqrt{200}}{8}\frac{n(r)}{\ln n(r)}\left[\frac{\overline{\rho}(r)}{\rho_{\mathrm{c}}}\right]^{-1/2} \tag{1}$$

correspond to different degrees of convergence depending on the value of the parameter $\kappa$. In this equation, $n(r)$ is the number of particles enclosed within the radius $r$ and $\overline{\rho}(r)/\rho_{\mathrm{c}}$ is the spherical density at this position in units of the critical value. Comparing the various resolutions of the Aquarius simulations, Navarro et al. (2010) showed that $\kappa = (7.0, 1.0, 0.4)$ correspond to deviations in the circular velocity profile of about (2.5, 10, 15) per cent, respectively. Here, we use $r_{\mathrm{conv}}(\kappa = 0.4)$ for each subhalo. We also define the tidal radius $r_{\mathrm{tidal}}$ of a subhalo as that which encompasses 95 per cent of the bound particles. The results from our definition show good agreement with the output from more sophisticated expressions for the tidal radius (Tormen, Diaferio & Syer 1998).

To make more direct comparisons to the satellite population of the MW, we have also run a semi-analytic model of galaxy formation for all the Aquarius haloes. This model is based on that originally developed by Kauffmann et al. (1999), Springel et al. (2001), De Lucia, Kauffmann & White (2004), Croton et al. (2006), De Lucia & Blaizot (2007) and later modified to describe more accurately processes on the scales of dwarf galaxies (Li, De Lucia & Helmi 2010). The implementation used here also includes recipes for stellar stripping and tidal disruption. The resulting satellite luminosity function agrees well with that of the MW as reported by Koposov et al. (2008) (see Section 3.3). Moreover, the internal properties of the satellites, such as scaling relations, metallicities and star formation histories, are in good agreement with those observed (for more details see Starkenburg et al. 2012).

## 3 RESULTS

### 3.1 About the density profiles

It has been already reported in the literature that the mass profiles of ΛCDM haloes deviate from the NFW functional form (Stoehr et al. 2002; Navarro et al. 2004; Merritt et al. 2005, 2006; Graham et al. 2006; Prada et al. 2006; Gao et al. 2008). Using the Aquarius simulations, Navarro et al. (2010) showed that a parametric model with a density profile with logarithmic slope described by a power law (Einasto profile) provides better fits for objects of virial mass $\sim 10^{12}\,\mathrm{M}_{\odot}$. The power index $\alpha$ adds another free parameter, therefore the fits are expected to improve. Nevertheless, it was shown by Springel et al. (2008) that even after fixing $\alpha = 0.16$ the Einasto profile still yields much better results. The nature of the shape parameter $\alpha$ has been recently investigated for isolated objects with masses in excess of $5 \times 10^{12}\,\mathrm{M}_{\odot}$ and the results suggest a deep connection with the pseudo-phase-space density distribution (Ludlow et al. 2011). For subhaloes, Springel et al. (2008) also showed that the mass profiles follow much closer the Einasto than the NFW model. For both models, the mass enclosed within the spherical radius $r$ can be written as

$$m(r) = 4\pi r_{-2}^3 \rho_{-2} g(r/r_{-2}), \tag{2a}$$

where $r_{-2}$ is the radius at which the logarithmic slope of the density profile reaches the isothermal value and $\rho_{-2}$ is the density at that

[1] In fact, shortly after we submitted our manuscript for publication, Wang et al. (2012) analysed the Millennium Simulation series and used the invariance of the scaled subhalo velocity function to argue that the absence of massive subhaloes might indicate that the MW is less massive than commonly assumed.

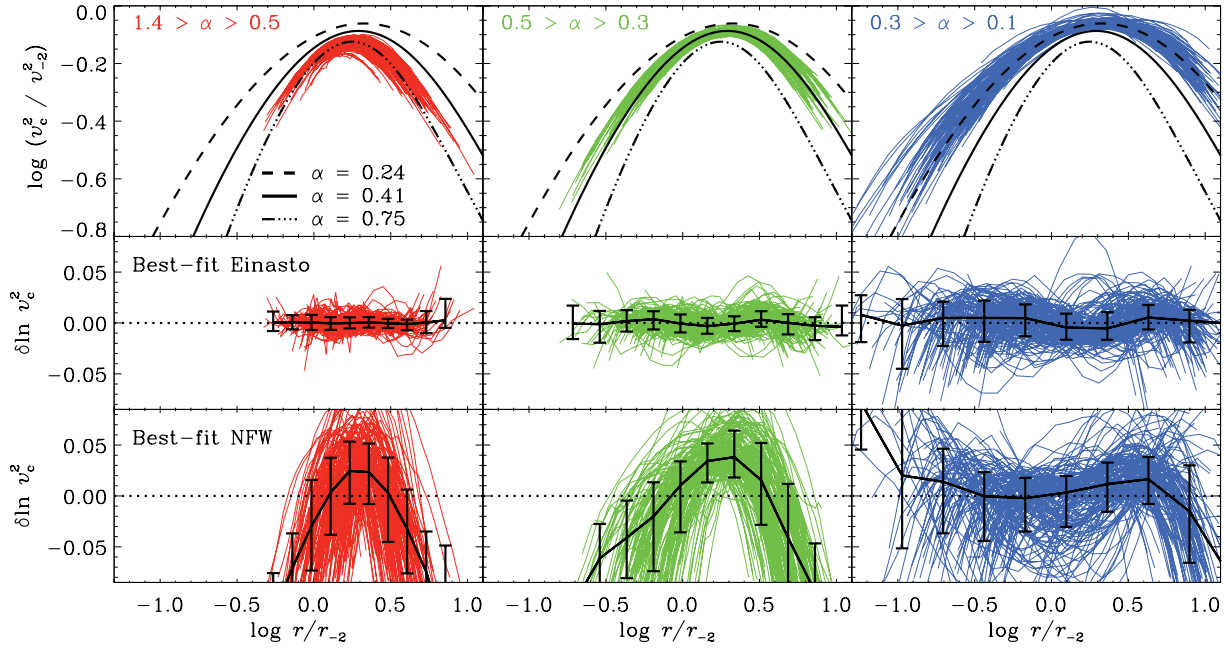


**Figure 1.** Spherically averaged circular velocity profiles $v_c^2(r) = Gm(r)/r$ for the subhaloes that are predicted to host stars by our semi-analytic model. Velocities have been scaled to $v_{-2}^2 \equiv 4\pi G\rho_{-2}r_{-2}^2$. As already reported in Stoehr et al. (2002) the velocity profiles of subhaloes tend to be more narrowly peaked than in the NFW form. The sample of subhaloes has been grouped according to the best-fitting value of $\alpha$, and plotted with different colours. The number of objects in each $\alpha$ bin is 154. An Einasto profile with the average value of $\alpha$ for each bin is overplotted, while the median $v_{\rm max}$ in each $\alpha$ bin is 13.6, 20.3 and 27 km s$^{-1}$ from left to right, and the $v_{\rm max}$ ranges given by the 68 per cent percentiles for each panel are (10, 26.2), (15.9, 26.2) and (20.5, 44.8) km s$^{-1}$, respectively. The residuals from the best-fitting Einasto (NFW) are shown in the middle (bottom) panel, and in general are consistent with zero for the Einasto profile and exhibit systematic deviations from zero for the NFW case. In the column $\langle\alpha\rangle = 0.24$ both models yield similar results, which is naturally expected since the NFW equivalent is reached with $\alpha = 0.22$. The systematic change of $r_{\rm conv}/r_{-2}$ with $\alpha$ is a consequence of setting the convergence parameter $\kappa$ to a fixed value.

position. The details of each model are inherited by the function $g$, which takes the form

$$g_{\rm NFW}(x) = 4\ln(1+x) - \frac{4x}{1+x} \tag{2b}$$

for the NFW profile, and

$$g_{\rm Einasto}(x) = \frac{1}{\alpha}\exp\left(\frac{3\ln\alpha + 2 - \ln 8}{\alpha}\right)\gamma\left(\frac{3}{\alpha}, \frac{2x^\alpha}{\alpha}\right) \tag{2c}$$

for the Einasto model. Here, $\gamma(a, x)$ is the lower incomplete gamma function. Although intrinsically different, these profiles resemble each other for $\alpha \approx 0.22$ in $0.01 \leq r/r_{-2} \leq 100$. That means that objects that have a shape parameter close to this value are well fitted by either model. Fig. 1 shows the spherically averaged circular velocity profiles $v_c^2 = Gm(r)/r$ for all the subhaloes that are predicted to host stars according to our semi-analytical model. In total we calculate 20 bins in the region $r_{\rm conv} \leq r \leq 0.9\, r_{\rm tidal}$; we use this upper cut-off to ensure that our fits are not driven by tidal effects. All objects have at least 200 particles, but generally significantly more than 1000. For each of the plotted subhaloes we calculate the merit function

$$E = \frac{1}{N_{\rm bins}}\sum_{i=1}^{N_{\rm bins}}\left[\ln v_c^2(r_i) - \ln v_{c,i}^2\right]^2, \tag{3}$$

and minimize it against the free parameters of each model. We have deliberately chosen to use the cumulative mass instead of the differential profile since it is less sensitive to the shot noise of each bin; as a consequence we can go to low number of particles, whenever the restriction $n(0.9\, r_{\rm tidal}) - n(r_{\rm conv}) \geq 200$ is met.

Fig. 1 shows the results of our fitting procedure. Here the subhaloes have been distributed in bins with equal number of objects (namely 154), and according to their best-fitting value of $\alpha$. The three different columns show the subhaloes that fall into each $\alpha$ bin, the average $\alpha$ within each bin is quoted in the top left-hand panel. Each curve in the top row has been conveniently normalized to a characteristic velocity $v_{-2}^2 \equiv 4\pi G\rho_{-2}r_{-2}^2$ and the characteristic radius $r_{-2}$. We have also overplotted the predicted Einasto profiles for the average $\alpha$. The middle panels show the residuals of the best-fitting Einasto for each subhalo, the thick line represents the median and $1\sigma$ equivalent dispersion. The residuals are consistent with zero indicating that the Einasto profile fits better than NFW (whose residuals are shown in the bottom panel), especially for large $\alpha$ values. Interestingly, for $\langle\alpha\rangle = 0.24$ the NFW model provides a good and comparable fit to the Einasto model (see the bottom right-hand panel). This is actually expected, since $\alpha = 0.22$ represents a model that nearly follows the NFW profile.

On average, lower mass subhaloes tend to have larger values of $\alpha$. However, this correlation has a large scatter; for instance, the maximum circular velocity for objects in the central panel of Fig. 1, i.e. those with $0.3 < \alpha < 0.5$, is in the range $10.5 < v_{\rm max}/{\rm km\,s^{-1}} < 48.2$.

### 3.2 MW's dSph constraints revisited

Wolf et al. (2010) have shown that the mass enclosed within the half-light radius $r_{1/2}$ of a dynamical system can be robustly determined as $m_{1/2} = 3G^{-1}\langle\sigma_v^2\rangle r_{1/2}$, without (precise) knowledge of its velocity anisotropy. Here, $\langle\sigma_v^2\rangle$ is the light-weighted average line-of-sight

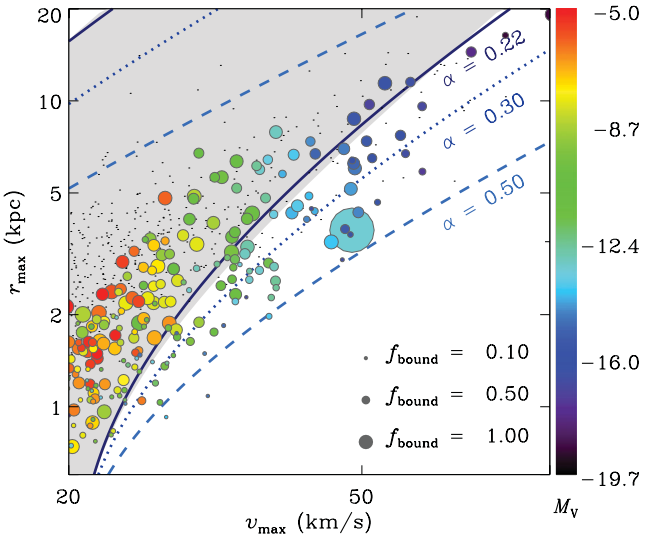


**Figure 2.** Constraints for the MW's dSphs using NFW (grey band) and Einasto (blue curves) profiles. Points are the results from the six Aquarius haloes, coloured according to their predicted luminosity and sized using the fraction of mass retained after infall. The cyan point at $v_{max} \sim 50$ km s$^{-1}$ represents a subhalo that underwent a merger with another substructure after infall, therefore increasing its mass. The black dots correspond to isolated haloes in the simulations.

velocity dispersion of the system. In the case of dSph galaxies, this effectively implies a measurement of the circular velocity at $r_{1/2}$, which therefore constrains the possible family of circular velocity curves for a given dark matter density profile. Following Boylan-Kolchin et al. (2011), we plot in Fig. 2 the $2\sigma$ constraints derived in this way for the nine most luminous dSph satellites of the MW (i.e. excluding the Sagittarius dwarf galaxy and the Small and Large Magellanic Clouds). Like Boylan-Kolchin et al. (2011) here we assume that these systems are embedded in NFW profiles, which leads to the grey band shown in the figure. This band is also nearly consistent with the masses enclosed within 300 pc as reported by Strigari et al. (2008): $2.5 \times 10^6 \leq m(300\ \mathrm{pc})/\mathrm{M}_\odot \leq 3.0 \times 10^7$.

The advantage of using this plot is that one can directly compare against the results extracted from ΛCDM simulations. The filled circles in Fig. 2 show the distribution of ($r_{max}$, $v_{max}$) measured directly from our simulations for the satellites hosting stars. The colours indicate the predicted luminosities and the sizes correspond to the bound mass fraction at present day, i.e. $f_{bound} = m(0)/m(z_{infall})$, where $z_{infall}$ is the lowest redshift at which the progenitor of a given subhalo was not associated with one of the main Aquarius haloes. Here, the values ($r_{max}$, $v_{max}$) have been corrected for softening length effects following the expressions given by Zavala, Springel & Boylan-Kolchin (2010). As highlighted in the Introduction, there are important differences in the location of the points from the simulations and those derived for the dSph satellites of the MW, which may lead to the conclusion that there is a significant problem with our currently preferred cosmological model.

However, this comparison may need to be revisited since we demonstrated in the previous section that an NFW profile is not expected to describe well the dark matter haloes of satellites in ΛCDM. Therefore, we have computed the family of ($r_{max}$, $v_{max}$) values that are consistent with the measurement of $v_c(r_{1/2})$ for the dSphs of the MW, but now we have considered Einasto profiles. The $2\sigma$ constraints are shown in Fig. 2. Given the freedom we have in choosing the extra parameter $\alpha$, we have plotted three different bands corresponding to $\alpha = (0.22, 0.30, 0.50)$. The $\alpha = 0.22$ (solid line) is consistent with the NFW predictions, as expected. For values of $\alpha \lesssim 0.5$ (dashed line) the constraints from observations actually overlap with those found in the simulations. This range of values of $\alpha$ lies well within the range observed in Fig. 1, since ∼2/3 of our sample has $\alpha < 0.5$.

From Fig. 2 we note that there is a correlation between the value of $\alpha$ and $f_{bound}$, i.e. the amount of stripping a subhalo has experienced. Very heavily stripped objects require, on average, higher $\alpha$, and deviate the most from NFW profiles. The black dots in this figure correspond to the location of isolated dark matter haloes in the same $v_{max}$ range as the satellites. This confirms that such isolated dark matter haloes are well fitted by NFW profiles, and that tidal stripping is acting on the subhaloes to change the shape of their circular velocity profile to the Einasto form (see also Hayashi et al. 2003).

The mismatch between the observations (with the assumption of NFW; Boylan-Kolchin et al. 2011) and the simulations is only partly alleviated with the use of an Einasto profile as shown in Fig. 2 The MW does not have many very luminous dwarf galaxy satellites. Brighter than Fornax ($M_V \sim -13.2$), only the Sagittarius dwarf and the Magellanic Clouds are known, and none is included in Fig. 2. According to our semi-analytic model such luminous objects would populate the upper right of this plot, i.e. $v_{max} \gtrsim 40$ km s$^{-1}$ and $r_{max} \gtrsim 2.5$ kpc. Therefore, in this region of the diagram, the mismatch between the observations and the simulations *has* to be entirely attributed to the absence of other bright dSphs in the MW, which is the point originally raised by Boylan-Kolchin et al. (2011). In other words, the lack of objects brighter (or more massive) than Fornax around the MW cannot be explained away through a change in the density profile of the dark matter subhaloes in the context of the ΛCDM model, unless these have been very heavily stripped. However, such massive subhaloes are typically accreted late, and hence have not suffered significant amounts of stripping. It is the region with $v_{max} \sim 20$–$40$ km s$^{-1}$, where we expect to find the subhaloes hosting most of the classical dSphs according to this plot, where the difference between assuming an NFW or an Einasto profile needs to be taken into account to bring the simulations in agreement with the observations.

### 3.3 Effects of the host halo mass

Springel et al. (2008) have shown that the mass function of dark matter haloes is independent of mass, i.e. it is self-similar. This implies that the number of subhaloes of a given mass scales directly with the mass of the host (although Gao et al. 2012 suggest that the slope is slightly larger for $10^{15}$ M$_\odot$ objects). Therefore, we can expect that, down to a certain scale, brighter or more massive central galaxies will host a larger number of satellites. This is indeed shown in the top panel of Fig. 3, where we have plotted the luminosity function of all Aquarius haloes. It is clear from this figure that this is the case, since the three heavier of the Aquarius haloes `Aq-A-2`, `Aq-C-2` and `Aq-D-2` have 57, 62 and 67 satellites, respectively, while the lightest, `Aq-B-2`, has only 36 satellites with $M_V \leq -5$, and hence has the shallowest luminosity function in the faint end. It is possible to show that a doubling of the mass of the host halo roughly leads to an increase by a factor of ∼2 in the number of satellites brighter than $M_V = -5$ (Starkenburg et al. 2012).

We thus explore the effect of host halo mass on the properties of our simulated satellites, by rescaling all haloes to a common value following Helmi, White & Springel (2003). Because of the

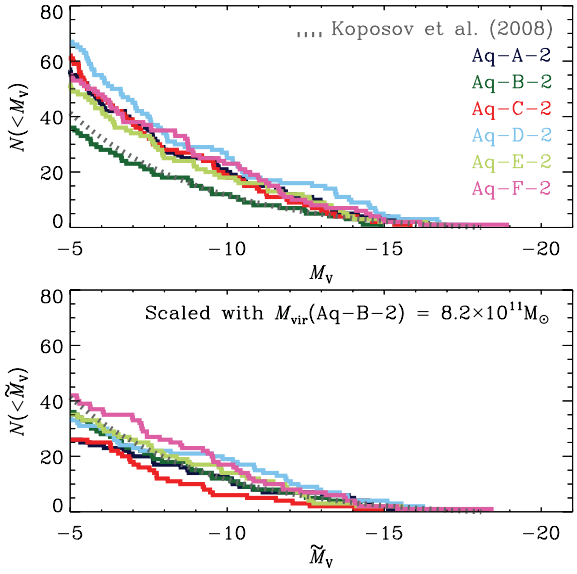


**Figure 3.** Luminosity function for the original Aquarius simulations (top) and once they have scaled to the mass of Aq−B−2 (bottom). For reference we have added the luminosity function derived by Koposov et al. (2008) for the MW. This takes into account incompleteness issues for satellites with $M_V > -11$, and for brighter objects it considers the average for the MW and M31. Although in the scaled version the simulations follow much more closely the observations, some differences remain in the number of satellites of a given luminosity.

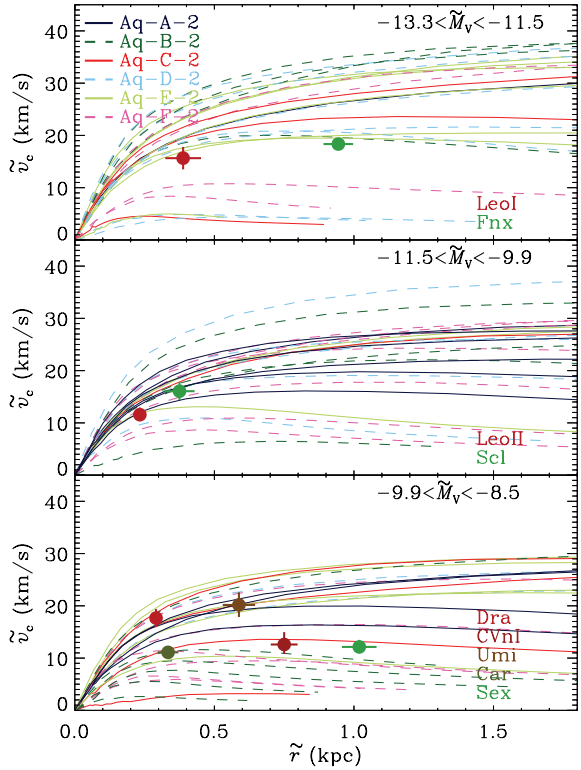


**Figure 4.** Circular velocity profiles for scaled subhaloes in three different luminosity bins, following the absolute magnitudes of the nine classical dSphs of the MW. The subhaloes are coloured according to the host halo they are associated with. This figure shows that the number of satellites per bin and the velocity profiles are consistent with the measurements obtained for the dSph.

scale-free nature of gravity, we may assume that if a halo of mass $M_{\rm Aq}$ is scaled to have a mass $M_{\rm MW}$ then the subhaloes' masses $m$ should be scaled as

$$\widetilde{m} = m\frac{M_{\rm MW}}{M_{\rm Aq}} \equiv \mu m. \tag{4a}$$

Naturally the distances will become

$$\widetilde{r} = \mu^{1/3} r, \tag{4b}$$

while the circular velocity profiles

$$\widetilde{v}_{\rm c} = \left(\frac{G\widetilde{m}}{\widetilde{r}}\right)^{1/2} = \mu^{1/3} v_{\rm c}. \tag{4c}$$

To determine the factor $\mu \equiv M_{\rm MW}/M_{\rm Aq}$, we need to specify $M_{\rm MW}$. As discussed in the Introduction, the value of the total mass of the MW is quite uncertain. However, motivated by the remarkable match between the luminosity function of Aq−B−2 and that of the MW (Koposov et al. 2008), we set $M_{\rm MW} = M_{\rm vir}$(Aq−B−2) $= 8.2 \times 10^{11}\,{\rm M}_\odot$.[2] This value is consistent with many recent studies using different techniques (e.g. Battaglia et al. 2005, 2006; Smith et al. 2007; Xue et al. 2008). This implies that the value of $\mu$ ranges from unity to 2.2 at most, which implies that distances and velocities in the scaled simulations will be at most decreased by a factor of 1.3.

We run our semi-analytic galaxy formation model now for the rescaled Aquarius simulations. The resulting luminosity function is shown in the bottom panel of Fig. 3, where the new predicted magnitudes are denoted by $\widetilde{M}_V$. It is evident from this figure that each halo now follows the MW's luminosity function much more closely. It is important to note that there is still some halo-to-halo dispersion, which can be attributed to the stochastic nature of the mass assembly of each object. That is, not all the galaxies with the same mass are expected to have the same number of satellites with the same luminosity, although some form of statistical equivalence should be present.

We now study more closely the circular velocity profiles of the subhaloes hosting satellites, since previous works have highlighted a discrepancy between the observations and the simulations (Boylan-Kolchin et al. 2011; Lovell et al. 2012). Fig. 4 shows the scaled circular velocity profiles for all the subhaloes hosting satellites with luminosities in the quoted range. As demonstrated in previous sections, we have also included the estimates for the nine most luminous dSphs of the MW following Wolf et al. (2010). The first conclusion is that our semi-analytic model places (satellite) galaxies of a given luminosity in the right mass (sub)haloes, since the amplitudes of the rotation curves in all cases are consistent with those observed. Secondly, the number of objects per luminosity bin is in good agreement with the number observed, as established in Fig. 3. For example, in the most luminous bin (top panel) the median number of bright satellites per halo is 3, while for intermediate luminosities it is 4 and for the faintest considered here, it is 4. We, however, emphasize that the range within a given luminosity bin is quite broad. For example, for the brightest bin, the scaled Aq−A−2 has just one satellite, while the scaled Aq−D−2 has seven. Such large variations are not unexpected, but stresses that strong conclusions cannot be drawn when the number of objects is so small as in the case of the bright end of the luminosity function.

[2] In this paper we denote $M_{\rm vir} = M_{200}$, i.e. the mass enclosed in a sphere with mean density 200 times the critical value.

**Table 1.** Statistical comparison of the nine most luminous classical dSphs with the simulated velocity profiles in Fig. 4.

| dSph | $N\sigma$ away | Observed $v_c(r_{1/2})$ | Median $v_c(r_{1/2})$ | med ($v_c$) $-1\sigma$ | med ($v_c$) $+1\sigma$ |
|---|---|---|---|---|---|
| Fnx | −0.72 | 18.3 | 25.4 | 6.0 | 32.0 |
| LeoI | −0.73 | 15.7 | 19.4 | 8.2 | 24.5 |
| Scl | −0.47 | 16.1 | 17.6 | 12.8 | 20.8 |
| LeoII | −1.03 | 11.6 | 14.2 | 11.9 | 16.8 |
| Sex | −0.22 | 12.1 | 16.4 | 4.4 | 25.3 |
| Car | −0.40 | 11.1 | 13.6 | 6.6 | 20.0 |
| Umi | +0.62 | 20.2 | 16.2 | 5.8 | 22.4 |
| CVnI | −0.23 | 12.6 | 16.3 | 5.1 | 23.0 |
| Dra | +1.03 | 17.7 | 13.6 | 6.7 | 17.6 |

The galaxies shown in the fainter two bins agree quite well with the predictions of our models. There is no systematic mismatch with the dSph circular velocity measurements at the half-light radius lying close to the median velocity profile of the simulated satellites. An apparent discrepancy is present in the most luminous bin $-13.2 \leq \widetilde{M}_V \leq -11.9$ in the sense that there is a larger number of subhaloes with circular velocities above the measured values for Fnx and LeoI than there is below. Nevertheless as discussed above, this comparison is limited by statistics and affected by stochastic aspects in the luminosity function.

We quantify this by comparing the observed value of the circular velocity at $r_{1/2}$ for each dSph, with the probability distribution function of $v_c$ calculated at the same radius using all the subhaloes that lie in the corresponding luminosity bin. We compute the median $v_c$ and two percentiles of the distribution, namely a lower (15.9 per cent) and an upper (84.1 per cent) value, which would correspond to $\pm 1\sigma$ in the case of a Gaussian. The results of this experiment are shown in Table 1 for the different satellites. Note that here we have translated the probability into an 'equivalent' $N\sigma$ away from the median. The table shows that all satellites are consistent with being drawn from the population of subhaloes hosting galaxies found in our simulations.

Thus far we have focused on the nine classical dSphs, and have excluded from the analysis the Sagittarius dwarf and the Magellanic Clouds. One of the questions originally posed by Boylan-Kolchin et al. (2012) is that there may be a hidden population of very massive subhaloes in the MW, since the circular velocities of the classical dwarfs are lower than those found for the nine most massive (at infall) subhaloes in any of the Aquarius simulations. So far we have shown that our model predicts the satellites of a given luminosity to be hosted in subhaloes of the right mass, when comparing to the classical dSph. However, we also need to explore what happens for systems brighter than Fnx, and whether we indeed expect a missing population from our models. As expected, the scaled Aquarius haloes show a diverse number of systems with $\widetilde{M}_V < -14$, ranging from two for `Aq-C-2` to five for `Aq-A-2`. A simple comparison to the MW satellite system would suggest that we cannot argue that there is a population of massive satellites that is missing.

This conclusion is also reached when considering $v_{\rm max}$ instead of luminosity. Although in general the most luminous objects are hosted by the most massive subhaloes, for $v_{\rm max} < 40$ km s$^{-1}$ and $\widetilde{M}_V > -14$ there is significant scatter, and objects as bright as Fnx are hosted in subhaloes with $v_{\rm max} \sim 5$–$35$ km s$^{-1}$ as shown in the top panel of Fig. 4. On the other hand, objects brighter than Fnx are generally hosted by subhaloes with $v_{\rm max} > 40$ km s$^{-1}$. We find

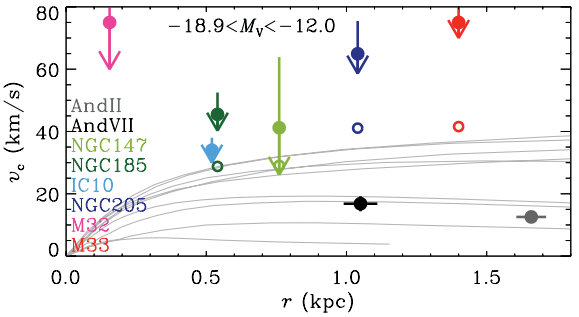


**Figure 5.** Circular velocities for the subhaloes present in halo `Aq-C-2` associated with satellites with luminosities $M_V \leq -12$. The symbols represent observations of the satellites of M31 in the same luminosity range. Open symbols represent the estimated dark matter contribution to $v_c(r)$ when the decomposition is available (see the text for details).

a median number of such subhaloes of two within 280 kpc from the centre for the scaled-down main Aquarius haloes, with three for `Aq-A-2` and none for `Aq-C-2`.

As suggested by multiple authors, the dark matter mass of M31 is almost twice that of the MW (e.g. Li & White 2008; Kallivayalil et al. 2009; Guo et al. 2010). This would imply that M31 should host more, and also brighter, satellites than the MW itself. This indeed appears to be the case, as M31 has eight satellites within 280 kpc that are brighter than LeoI ($M_V = -11.9$) compared to two (or five when Sgr and the Magellanic Clouds are included) for the MW.

Aquarius halo `Aq-C-2` has $M_{\rm vir} = 1.77 \times 10^{12}$ M$_\odot$ which is ∼2.2 times larger than our candidate for the MW, making this object a good match for M31. In Fig. 5, we show the velocity profiles of all the nine satellites in `Aq-C-2` with $M_V \leq -12$. We have also included measurements for M31's satellites with luminosities in that range. It is important to bear in mind that these measurements have been derived using a variety of methods that range from H I rotation curves for IC10 (Wilcots & Miller 1998) and M33 (Corbelli 2003), to three integral dynamical modelling for NGC 147, NGC 185 and NGC 2005 (De Rijcke et al. 2006). For the dSphs AndII and AndVII the method presented by Wolf et al. is used to estimate $v_c(r_{1/2})$ (Kalirai et al. 2010), while for M32 the mass is derived through Jeans modelling (Magorrian & Ballantyne 2001). Many of these bright dwarf galaxies are not as dark matter dominated within the region populated by the stars as the dSph, and hence a direct comparison to the circular velocity of the subhaloes is not quite correct. For example, for NGC 147, NGC 185 and NGC 2005, the dark matter content is estimated to be 50, 40 and 40 per cent, respectively (De Rijcke et al. 2006). The open symbols in Fig. 5 thus correspond to the dark matter contribution to the circular velocity as estimated by these authors, while the solid points represent the total enclosed mass at the given radius. Clearly for M32, a very compact dwarf elliptical, the shown circular velocity is also an upper limit for the dark matter contribution.

This comparison shows that the velocity profiles for our most luminous satellites in `Aq-C-2` are very consistent with the observations of the dwarfs in M31 over a similar luminosity range. We must therefore conclude that there is no evidence of a missing population of very massive dark satellites.

## 4 DISCUSSION AND CONCLUSIONS

We have used the state of the art cosmological *N*-body simulations of MW-like dark matter haloes of the Aquarius project, supplemented

with a semi-analytic galaxy formation model, to study the dynamical properties of the satellite population in the Local Group.

We have found that the mass profiles of the subhaloes associated with bright satellites according to our model deviate from the standard NFW form (see also Stoehr et al. 2002), and that Einasto profiles provide much better fits. The shape parameter $\alpha$ exhibits a correlation with the amount of mass stripped since the time of accretion, indicating that tidal effects may be responsible for the changes in the profiles of dark matter haloes once they become satellites (Hayashi et al. 2003).

The comparison of our models to current measurements of the mass enclosed within the half-mass radius for the classical dSphs suggests that they are embedded in dark matter haloes of $v_{\rm max} \sim$ 10–30 km s$^{-1}$ with $\alpha \sim 0.2$–0.5. In principle, this prediction for the values of the shape parameter $\alpha$ could be tested observationally. However, this requires very extensive sampling of the kinematics of stars near the centre of the dwarf galaxies. It is also necessary to perform more sophisticated dynamical models that are free of assumptions regarding the velocity anisotropy of the systems. For example, Schwarzschild models of the Sculptor dSph constrain the inner logarithmic slope of the dark matter density profile to be $\mathrm{d}\log\rho/\mathrm{d}\log r > -1.5$ (Breddels et al. 2012). Better constraints could be obtained if the sample size were increased by a factor of $\sim$10.

We have also shown that the number and internal dynamics of the classical dSph in the MW are consistent with the predictions of the $\Lambda$CDM model, if the MW's mass is $\sim 8 \times 10^{11}\,\mathrm{M}_{\odot}$. This value well within the range measured using the dynamics of stellar tracers, but suffers from significant uncertainties. However, it is important to note that this low value lowers the probability of a galaxy like the MW to host two satellites as bright as the Small and Large Magellanic Clouds (Boylan-Kolchin et al. 2010; Busha et al. 2011b), although such systems appear to be rare in any case, as shown by Liu et al. (2011) using the Sloan Digital Sky Survey.

We have also found significant scatter in the number of subhaloes expected to host bright satellites for the Aquarius haloes, even when scaled to a common mass of $8 \times 10^{11}\,\mathrm{M}_{\odot}$. For example, the scaled `Aq-A-2` has five satellites brighter than Fornax, while the scaled `Aq-C-2` has only two (making it consistent with our Galaxy). Therefore, care should be taken to draw strong conclusions from this region of the luminosity function since the number of objects is small and heavily influenced by the host mass as well as by stochastic effects associated with particular histories. Another example that emphasizes this point is given by M31, which plausibly is nearly a factor of 2 more massive than the MW and also has a larger number of bright satellites. Just like for the MW, our models for the satellite population of M31 are consistent with the observational constraints on the internal dynamics of the brighter satellites, after taking the differences in host mass into account.

A similar conclusion was reached by Wang et al. (2012) in a paper submitted shortly after ours, and based on the Millennium Simulation series. These authors show that the cumulative number of subhaloes with a given peak circular velocity depends roughly linearly on host halo mass, and that it is a highly stochastic quantity. In fact, once normalized to the mass of the host, this function is close to Poissonian. Based on this result, they conclude that $\sim$46 per cent of the haloes with $M = 10^{12}\,\mathrm{M}_{\odot}$ have no more than three subhaloes more massive than $v_{\rm max} = 30$ km s$^{-1}$, and that the percentage increases to $\sim$61 per cent for haloes with $M = M(\mathtt{Aq\text{-}B\text{-}2}) = 8.2 \times 10^{11}\,\mathrm{M}_{\odot}$, in good agreement with our own inferences. Hence we must conclude that we have found no evidence of a missing massive satellite problem in the Local Group.

## ACKNOWLEDGMENTS

The Aquarius simulations have been run by the VIRGO consortium, and we are very thankful to this collaboration, and especially indebted to Volker Springel. We are very grateful to Gabriella De Lucia and Yang-Shyang Li in relation to the semi-analytic model of galaxy formation, and to Simon White, Mike Boylan-Kolchin and the referee for a critical reading of the manuscript. AH gratefully acknowledges financial support from the European Research Council under ERC-Starting Grant GALACTICA-240271. ES is supported by the Canadian Institute for Advanced Research (CIfAR) Junior Academy and a Canadian Institute for Theoretical Astrophysics (CITA) National Fellowship.

## REFERENCES

Battaglia G. et al., 2005, MNRAS, 364, 433
Battaglia G. et al., 2006, MNRAS, 370, 1055
Benson A. J., Lacey C. G., Baugh C. M., Cole S., Frenk C. S, 2002, MNRAS, 333, 177
Boylan-Kolchin M., Springel V., White S. D. M., Jenkins A, 2010, MNRAS, 406, 896
Boylan-Kolchin M., Bullock J. S., Kaplinghat M., 2011, MNRAS, 415, L40
Boylan-Kolchin M., Bullock J. S., Kaplinghat M., 2012, MNRAS, 422, 1203
Breddels M. A., Helmi A., van den Bosch R. C. E., van de Ven G., Battaglia G., 2012, in Reylé C., Robin A., Schultheis M., eds, EPJ Web Conf., Vol. 19, Assembling the Puzzle of the Milky Way. EDP Sciences, p. 03009
Bullock J. S., Kravtsov A. V., Weinberg D. H., 2000, ApJ, 539, 517
Busha M. T., Weschler R. H., Behroozi P. S., Gerke B. F., Klypin A. A., Primack J. R., 2011a, ApJ, 743, 40
Busha M. T., Weschler R. H., Behroozi P. S., Gerke B. F., Klypin A. A., Primack J. R., 2011b, ApJ, 743, 117
Corbelli E., 2003, MNRAS, 342, 199
Couchman H. M. P., Rees M. J., 1986, MNRAS, 221, 53
Croton D. J. et al., 2006, MNRAS, 365, 11
De Lucia G., Blaizot J., 2007, MNRAS, 375, 2
De Lucia G., Kauffmann G., White S. D. M., 2004, MNRAS, 349, 1101
De Rijcke S., Prugniel P., Simien F., Dejonghe H., 2006, MNRAS, 369, 1321
Di Cintio A., Knebe A., Libeskind N. I., Yepes G., Gottlöber S., Hoffman Y., 2011, MNRAS, 417, L74
Di Cintio A., Knebe A., Libeskind N. I., Brook C., Yepes G., Gottlöber S., Hoffman Y., 2012, preprint (arXiv:1204.0515)
Efstathiou G., 1992, MNRAS, 256, 43p
Font A. S. et al., 2011, MNRAS, 417, 1260
Gao L., Navarro J. F., Cole S., Frenk C. S., White S. D. M., Springel V., Jenkins A., Neto A. F., 2008, MNRAS, 387, 536
Gao L., Navarro J. F., Frenk C. S., Jenkins A., Springel V., White S. D. M., 2012, MNRAS, 425, 2169
Gnedin O. Y., Brown W. R., Geller M. J., Kenyon S. J., 2010, ApJ, 720, L108
Graham A. W., Merrit D., Moore B., Diemand J., Terzić B., 2006, AJ, 132, 2701
Guo Q., White S., Li C., Boylan-Kolchin M., 2010, MNRAS, 404, 1111
Guo Q. et al., 2011, MNRAS, 413, 101
Hayashi E., Navarro J. F., Taylor J. E., Stadel J., Quinn T., 2003, ApJ, 584, 541
Helmi A., White S. D. M., Springel V., 2003, MNRAS, 339, 834
Kalirai J. S. et al., 2010, ApJ, 711, 671
Kallivayalil N., Besla G., Sanderson R., Alcock C., 2009, ApJ, 700, 924
Kauffmann G., White S. D. M., Guiderdoni B., 1993, MNRAS, 264, 201

Kauffmann G., Colberg J. M., Diaferio A., White S. D. M., 1999, MNRAS, 303, 188
Klypin A., Kravtsov A. V., Valezuela O., Prada F., 1999, ApJ, 522, 82
Kochanek C. S., 1996, ApJ, 457, 228
Koposov S. et al., 2008, ApJ, 686, 279
Li Y.-S., White S. D. M., 2008, MNRAS, 384, 1459
Li Y.-S., Helmi A., De Lucia G., Stoehr F., 2009, MNRAS, 397, L87
Li Y.-S., De Lucia G., Helmi A., 2010, MNRAS, 401, 2036
Liu L., Gerke B. F., Wechsler R. H., Behroozi P. S., Busha M. T., 2011, ApJ, 733, 62
Lovell M. R. et al., 2012, MNRAS, 420, 2318
Ludlow A. D., Navarro J. F., White S. D. M., Boylan-Kolchin M., Springel V., Jenkins A., Frenk C. S, 2011, MNRAS, 415, 3895
Macciò A. V., Kang X., Fontanot F., Somerville R., Koposov S., Monaco P., 2010, MNRAS, 402, 1995
Madau P., Diemand J., Kuhlen M., 2008, ApJ, 679, 1260
Magorrian J., Ballantyne D., 2001, MNRAS, 322, 702
Merritt D., Navarro J. F., Ludlow A., Jenkins A., 2005, ApJ, 624, L85
Merritt D., Graham A. W., Moore B., Diemand J., Terzić B., 2006, AJ, 132, 2685
Moore B., Ghigna S., Governato F., Lake G., Quinn T., Stadel J., Tozzi P., 1999, ApJ, 524, L19
Navarro J. F., Frenk C. S., White S. D. M., 1996, ApJ, 462, 563
Navarro J. F., Frenk C. S., White S. D. M., 1997, ApJ, 490, 493
Navarro J. F. et al., 2004, MNRAS, 349, 1039
Navarro J. F. et al., 2010, MNRAS, 402, 21
Okamoto T., Frenk C. S., 2009, MNRAS, 399, L174
Power C., Navarro J. F., Jenkins A., Frenk C. S., White S. D. M., Springel V., Stadel J., Quinn T., 2003, MNRAS, 338, 14
Prada F., Klypin A. A., Simonneau E., Betancort-Rijo J., Patiri S., Gottlöber S., Sanchez-Conde M. A, 2006, ApJ, 645, 1001
Reed D. S., Koushiappas S. M., Gao L., 2011, MNRAS, 415, 3177
Sakamoto T., Chiba M., Beers T. C., 2003, A&A, 397, 899
Smith M. C. et al., 2007, MNRAS, 379, 755
Somerville R. S., 2002, ApJ, 572, L23
Springel V., White S. D. M., Tormen G., Kauffmann G., 2001, MNRAS, 328, 726
Springel V. et al., 2008, MNRAS, 391, 1685
Starkenburg E. et al., 2012, preprint (arXiv:1206.0020)
Stoehr F., White S. D. M., Tormen G., Springel V., 2002, MNRAS, 335, L84
Strigari L. E., Bullock J. S., Kaplinghat M., Simon J. D., Geha M., Willman B., Walker M. G., 2008, Nat, 454, 1096
Stringer M., Cole S., Frenk C. S., 2010, MNRAS, 404, 1129
Thoul A. A., Weinberg D. H., 1996, ApJ, 465, 608
Tormen G., Diaferio A., Syer D., 1998, MNRAS, 299, 728
Vogelsberger M., Zavala J., Loeb A., 2012, MNRAS, 423, 3740
Walker M. G., Mateo M., Olszewski E. W., Peñarrubia J., Wyn Evans N., Gilmore G., 2009, ApJ, 704, 1274
Wang J., Frenk C. S., Navarro J. F., Gao L., Sawala T., 2012, MNRAS, 424, 2715
Watkins L. L., Evans N. W., An J. H., 2010, MNRAS, 406, 264
Wilcots E. M., Miller B. W., 1998, AJ, 116, 2363
Wilkinson M. I., Evans N. W., 1999, MNRAS, 310, 645
Wolf J., Martinez G. D., Bullock J. S., Kaplinghat M., Geha M., Muñoz R. R., Simon J. D., Avedo F. F., 2010, MNRAS, 406, 1220
Xue X. X. et al., 2008, ApJ, 684, 1143
Zavala J., Springel V., Boylan-Kolchin M., 2010, MNRAS, 405, 593

This paper has been typeset from a TEX/LATEX file prepared by the author.